Published in final edited form as:
Brain Stimul. 2012 July ; 5(3): 369–377. doi:10.1016/j.brs.2011.05.002.

Current steering to activate targeted neural pathways during deep brain stimulation of the subthalamic region

Ashutosh Chaturvedi[a,b], **Thomas J. Foutz**[a,b], and **Cameron C. McIntyre**[a,b,*]

[a]Department of Biomedical Engineering, Cleveland Clinic Foundation, Cleveland, OH, USA

[b]Department of Biomedical Engineering, Case Western Reserve University, Cleveland, OH, USA

Abstract

Deep brain stimulation (DBS) has steadily evolved into an established surgical therapy for numerous neurological disorders, most notably Parkinson's disease (PD). Traditional DBS technology relies on voltage-controlled stimulation with a single source; however, recent engineering advances are providing current-controlled devices with multiple independent sources. These new stimulators deliver constant current to the brain tissue, irrespective of impedance changes that occur around the electrode, and enable more specific steering of current towards targeted regions of interest. In this study, we examined the impact of current steering between multiple electrode contacts to directly activate three distinct neural populations in the subthalamic region commonly stimulated for the treatment of PD: projection neurons of the subthalamic nucleus (STN), globus pallidus internus (GPi) fibers of the lenticular fasiculus, and internal capsule (IC) fibers of passage. We used three-dimensional finite element electric field models, along with detailed multi-compartment cable models of the three neural populations to determine their activations using a wide range of stimulation parameter settings. Our results indicate that selective activation of neural populations largely depends on the location of the active electrode(s). Greater activation of the GPi and STN populations (without activating any side-effect related IC fibers) was achieved by current steering with multiple independent sources, compared to a single current source. Despite this potential advantage, it remains to be seen if these theoretical predictions result in a measurable clinical effect that outweighs the added complexity of the expanded stimulation parameter search space generated by the more flexible technology.

Keywords

Deep brain stimulation; computational modeling; neural activation; Parkinson's disease; current controlled stimulation; current steering

*Corresponding author: Cameron C. McIntyre, Department of Biomedical Engineering, Cleveland Clinic Foundation, 9500 Euclid Avenue ND-20, Cleveland, Ohio 44195, Telephone: (216) 445-3264, Fax: (216) 444-9198, mcintyc@ccf.org.

Conflict of Interest

Paid consultancy for A.C. and C.C.M. (Intelect Medical Inc.); A.C., T.J.F., and C.C.M. (Boston Scientific Neuromodulation Corp.)

Introduction

Deep brain stimulation (DBS) of the subthalamic region is an established therapy for medically intractable Parkinson's disease (1, 2). The basic goal is to stimulate targeted brain regions (eliciting a therapeutic response) while minimizing stimulation of non-target brain regions (responsible for side effects). Stimulation is delivered by an implanted pulse generator (IPG) through electrodes implanted in subcortical structures. However, direct stimulation of the targeted brain tissue can be hindered by inaccurate electrode placement or by limitations in the IPG/electrode to generate the necessary electric field for optimal therapeutic benefit (3, 4).

DBS surgeries require precise targeting of the electrode in the brain; however, even with the most advanced surgical techniques, spatial deviations of electrode placement can occur. Subcortical structures can shift by an average 2 mm (4 mm in rare occasions) over the course of a DBS surgery (5–8). During bilateral implantation, insertion of the initial lead can affect the location of the contralateral lead by up to 2.5 mm (9). While small, these deviations in electrode placement may limit the ability of the stimulators to selectively activate the target brain region.

Historically, clinical DBS IPGs have been developed as voltage-controlled devices with a single stimulation source. However, DBS technology is rapidly evolving into current-controlled devices with multiple independent current sources. This transition to current-controlled stimulation will allow stimulators to create a more consistent voltage distribution within brain tissue (10), regardless of encapsulation changes around the electrode or changes in electrode impedance (11). Independent current sources will enable devices to use a wider array of cathode/anode stimulation combinations while varying the stimulation amplitudes across active contacts, essentially steering the electric fields (4). This could represent a potential advantage for patients with less than optimal electrode placements, as generally, patients who undergo DBS surgery do not have their electrodes removed and repositioned, unless stimulation through every contact is ineffective. Additionally, patients with less than optimal electrode placement are often forced to undergo extensive programming sessions months or years after surgery in attempts to adjust their clinical stimulation settings to provide maximal therapeutic benefit.

The underlying hypothesis of this study is that current-controlled devices with independent current sources should increase the ability of clinicians to better tailor stimulation to an individual patient. We propose that a more detailed understanding of the neural response to multipolar DBS may guide the development of this technology and potentially increase its clinical benefit. In this study, we explore the ability of current steering to activate three distinct neural populations in the subthalamic region: 1) projection neurons of the subthalamic nucleus (STN), 2) globus pallidus internus (GPi) fibers of passage in the lenticular fasciculus, and 3) internal capsule (IC) fibers of passage. While numerous additional neural populations exist within the subthalamic region, we have selected these three as logical candidates representing therapeutic targets (STN and GPi) and a side effect region (IC).

Materials and methods

Predictions of neural activation in response to DBS were performed using a detailed computational model of STN DBS that included three major components: 1) 3D representation of the DBS electrode within the subthalamic nucleus, 2) 3D reconstructions of STN, GPi, and IC populations, and 3) finite element models of the electric fields generated by a wide range of stimulation settings. The numbers of active cathodic and/or

anodic contacts, as well as the current stimulus amplitude delivered through each contact, were varied, and the relative percentages of neural activation across the three populations were compared.

Anatomical model and electrode position

The anatomical model was defined by magnetic resonance imaging (MRI) human data, as described in our previous work (12). All modeling results were generated within the context of an atlas brain, which consisted of a T1 MRI and a diffusion tensor imaging (DTI) dataset (13). The DTI was used to estimate 3D tissue anisotropy and inhomogeneity in the region of interest surrounding the STN (12, 14, 15). Three-dimensional representations of relevant anatomical nuclei (STN, GPi, and thalamus) provided a visual frame of reference for the figures.

A virtual electrode was created based on the dimensions of a Medtronic 3389 DBS lead (Medtronic Inc., Minneapolis MN). Contact 1 of the model electrode was located at the centroid of the STN, and the arc and collar angles of its trajectory were 20° and 100°, respectively, in an AC/PC-based coordinate system (Fig. 1B). The anatomical nuclei, DTI dataset, and virtual electrode position were loaded into a common 3D visualization and simulation environment for analysis (SCIRun/BioPSE, Scientific Computing and Imaging Institute, University of Utah, Salt Lake City, UT).

Neuron models

This study focused on the activation response of three different neural populations: 1) STN projection neurons, 2) GPi fibers of passage, and 3) IC fibers of passage. Three subtypes of the STN projection neuron geometry was implemented, each with an identical soma-dendritic architecture, but with three different axon trajectories projecting to the globus pallidus (16, 17) (Fig. 1G). The somas of the STN projection neurons were placed randomly within the atlas-defined borders of the subthalamic nucleus, with the constraint that their axons terminated in the globus pallidus (Fig. 1H). This process produced a total of 80 STN projection neurons once we removed any neurons with processes passing through the electrode. Due to their close proximity to the active DBS electrode contacts, these projection neurons required explicit modeling of their soma-dendritic architecture within the STN. The dendritic geometry and axonal trajectories were based on microscopic tracing studies in non-human primates (17).

The trajectories of the GPi fibers of passage were based on detailed anatomical reconstructions of individual pallidal neurons (18). The basic GPi axonal trajectory originated in the GPi, traversed dorsal to the STN, and ultimately projected to the thalamus (Fig. 1E). The population of 100 GPi fibers corresponded to the general trajectory of the lenticular fasciculus (Fig. 1F).

The anatomical geometry of the IC fibers was defined via streamline tractography within SCIRun/BioPSE (19) using the DTI dataset accompanying our atlas brain (13). Two hundred fibers were defined from a rectangular seed region, approximately 5 × 1 × 2 mm in size, positioned lateral to the STN to generate a dense population within the IC (Fig. 1C–D) (20). It should be noted that a similar streamline tractography process was also attempted to define the lenticular fasiculus, but was deemed unreliable due to the large number of crossing fibers within the region of interest.

We created populations of multi-compartment cable models representing STN projection neurons, GPi fibers of passage, and IC fibers of passage (Figure 1). These populations were distributed randomly within anatomically realistic regions relative to the brain atlas. Active membrane dynamics were incorporated into the axon of each neuron model. Since

morphological data on these axons are limited, and to enable consistent comparison between stimulation induced activation of the different neural populations, every axon was implemented with the same model parameters (5.7 μm outer diameter of the myelin) (21).

STN neurons are tonically active, making the extracellular activation threshold time dependent (i.e. relative to the ongoing intrinsic activity). Therefore, to quantify stimulation threshold for the purposes of this study, the soma-dendritic compartments of the STN models were simplified to have passive membrane properties only (i.e. leakage conductance in parallel with membrane capacitance). This simplification resulted in a stable rest potential for the STN neuron and is justified because action potential initiation during extracellular stimulation of projection neurons occurs in the axon (16, 22–24). This simplification enabled us to consistently compare activation thresholds of the different neural populations, as they all had the same axon membrane dynamics. Furthermore, we previously demonstrated similar activation thresholds for STN neurons with and without active membrane dynamics in the soma-dendritic compartments (25).

Electric field model

The voltage distribution generated in the brain during DBS, in response to over 400 different stimulation settings, was simulated using a finite element model (FEM) (12, 15, 20). A multi-resolution finite element mesh of the DBS electrode and surrounding tissue medium was constructed using FEMLAB 3.1 (Comsol Inc., Burlington, MA), which consisted of over 4.2 million nodes. The FEM mesh was imported into SCIrun/BioPSE and co-registered with the anatomical model and DTI atlas brain (12). Conductivity tensors were estimated from each voxel of the DTI (14) and interpolated onto the FEM mesh. The Poisson equation was solved in 3D to determine the electric field generated by multiple electrode contacts during current-controlled stimulation (4). The virtual DBS electrode generated a biphasic, charge-balanced, 100 μs pulse-width rectangular waveform, representative of the Boston Scientific Precision IPG (Boston Scientific, Natick, MA).

Activation of the neural populations

Our primary goal was to investigate the impact of steering current (between electrode contacts) on the threshold for action potential generation in each of the three neural populations. Voltage solutions from each stimulation setting were linearly interpolated from the FEM onto the center of every subcellular compartment within each neuron model. Simulations of the neural response to the applied electric field were performed in NEURON 6.2 (26). Activation for each of the 380 model neurons to a single stimulus pulse was defined as the generation of a stimulation-induced propagating action potential along the entire length of the axon.

Finally, we redistributed all neuron trajectories four additional times for all three neural population groups (GPi, STN, and IC) using the same methodologies described above, to account for anatomic variability in neuron locations. The addition of multiple sets of neural populations also allowed us to perform a paired *t*-test to assess statistical significance in differences between activation when comparing independent current sources with single-source stimulation. To simplify data presentation, all the figures presented describe results using the original set of neuron trajectories; whereas, Table 1 summarizes the results from all five sets of neuron locations. The maximum average selective activation of both therapeutic targets is reported in Table 1. The combined results describe the stimulation setting at which the percentages of activated neurons are maximal when averaged together.

Results

This study was undertaken with the basic assumption that optimal therapeutic benefit from DBS is achieved when activation of target neural populations is maximized, and the activation of side-effect neural populations is minimized. Within the context of this theoretical study, our target neural population was composed of STN projection neurons and GPi fibers of passage. The IC fibers of passage were defined as the deleterious side-effect neural population. Our results outline the impact of searching through the complex parameter space of a DBS device with current steering capabilities.

Monopolar stimulation

Numerous clinical reports have concluded that the best therapeutic benefits from DBS for PD are achieved with electrode contacts located at or near the dorsal border of the STN. Therefore, we designated contact 2 as the principal therapeutic contact of interest given our electrode location within the anatomy (Fig. 1). Monopolar stimulation with contact 2 was able to activate neurons from each of the three neural populations. Figure 2 provides an illustrative example of neural activation from a single set of neuron locations generated by a cathodic −6 mA stimulus delivered through contact 2, activating 43% of the STN neurons, 62% of the GPi fibers of passage, and 5% of the IC axons.

Our primary interest was to identify techniques that maximized activation of target neural populations without activating side-effect populations. The model predicted the maximum amplitude sub-threshold for IC fiber activation to be approximately −5 mA with monopolar stimulation through contact 2. This stimulation setting activated on average 47% STN projection neurons and 39% GPi fibers of passage when considering all five sets of neuron locations (Table 1). We defined this monopolar activation profile as the “gold-standard” and compared it to a range of single-source bipolar and multi-source current steering stimulation strategies.

Bipolar stimulation

A single source DBS device enables the possibility of setting two or more contacts to the same amplitude (i.e. double monopolar) or setting one contact to be an anode and others to be a cathode. The most common clinical implementation of this concept is bipolar stimulation with an adjacent anode and cathode. However, given the placement of our model DBS electrode in the atlas brain, the use of multiple cathodes represented a more effective strategy for stimulating the target neural populations (Table 1). Stimulation with contacts 2 and 3 both set to −3 mA activated on average just over half of the STN and nearly 45% of the GPi axons before spreading stimulation into the IC. This was considered a more favorable setting than the “monopolar gold-standard” since there was slightly increased activation of the targeted neural populations, and no IC activation. Further efficacy was achieved using current steering with independent current sources (contact 2 at −4 mA and contact 3 at −2 mA), increasing STN activation to 55% and GPi activation to 51%, with no IC activation (Table 1). After performing a *t*-test, using a p-value of 0.05, and comparing results from 5 different neuron distributions, we found there was a statistically significant difference in therapeutic activation when using current steering instead of a single-source monopolar or two-cathode configuration.

Activation maps for both therapeutic neural populations during current steering between two adjacent contacts are displayed in Figure 3. There was no IC activation when using stimulation settings inside the dashed lines. We stimulated each active contact pair with amplitudes ranging from a maximal cathodic current of −5 mA to a maximal anodic current +5 mA (1 mA resolution). In situations where the different electrode contacts had an

imbalance between anodic and cathodic current, the boundary conditions of the model accounted for the presence of the IPG as an additional return electrode. These results demonstrate the greater stimulation potency of cathodic stimulation, relative to anodic stimulation. However, as noted in previous theoretical studies anodic stimulation can be an effective strategy for recruiting local projection neurons with extracellular electrodes (27).

Additional current steering permutations

A wide range of activation percentages for different neural populations could be achieved via independent current steering between adjacent electrode contacts (Fig. 3). However, future technology will also enable independent activation of three (or more) electrode contacts. Figure 4 shows an example of transitioning current between contacts 1, 2, and 3. These results illustrate that tripolar configurations were able to generate some degree of selective activation of targeted neural populations. However, tripolar configurations were no more effective than bipolar configurations for the electrode location and target neural populations examined in this study.

Electrode placement sensitivity

Based on our previous experience developing computational models for DBS applications, we believe that defining the precise implanted electrode position in the brain represents one of the largest sources of error. Therefore, we investigated how changes in the electrode location affected selective stimulation of the neural populations during current steering (Figure 5). First, starting from the default electrode location, we perturbed the electrode ± 2 mm in 0.5 mm increments within the transverse (axial) xy-plane. At each electrode location, contacts 2 and 3 were set to ± 5 mA (1 mA increments). Next, we determined the maximum average activation of our therapeutic targets (percent GPi axons and STN neurons) with no IC activation at each lead location (Figure 5). Not surprisingly, as the electrode was placed farther away from the IC fibers of passage (i.e. more medial and/or posterior), we observed a higher therapeutic selectivity, up to a maximum average of 81%. Interestingly, current steering can achieve a similar therapeutic activation at many different electrode locations. For example, the maximum average therapeutic activation is similar when the electrode lead was placed 1.5 mm medial or 1.5 mm posterior from the default location (Figure 5).

Discussion

The goal of this study was to evaluate the ability of current steering technology to improve DBS activation selectivity in targeted neural populations. We used a highly detailed electric field model coupled to 3D neuron models with anatomically realistic geometries and membrane dynamics. We focused on activation of three different neural populations (STN projection neurons, GPi fibers of the lenticular fasciculus, and IC fibers of passage), and quantified their activation by performing a comprehensive search through various stimulation parameter options. Our results show that current steering can be an effective technique to bias activation toward specific neural populations. However, introduction of current steering technology into DBS practice broadens the search for an optimal stimulation setting in each patient.

Current steering

Our computational model demonstrates the ability of current steering to activate different proportions of three distinct neural populations, without changing the implanted electrode position. Once explicit neural targets are defined, current steering may represent a strategy to overcome small errors in surgical placement of the electrode. Alternatively, implantation of electrodes with a large number of small surface area contacts could also help focus stimulation on a target area. However, the use of small electrode contacts may introduce

limitations in the spatial extent of stimulus spread due to limitations on safe charge injection limits (32). Therefore, current steering between traditionally sized contacts provides additional flexibility to choose alternate stimulation parameters that may inject less total current into the tissue.

While current steering has the potential advantage of finer control over the volumes of tissue activated, it comes at the cost of an expanded search space, potentially increasing the difficulty of patient programming. The current state-of-the-art methodology for clinical DBS programming is performed without much visual or computational guidance, and relies primarily on clinical intuition. This traditional approach often requires multiple programming sessions with the patient, and still requires an experienced DBS clinician to achieve an optimal result (33). We have proposed that visualization software could help guide clinicians with patient-specific computational models of activation during programming sessions (34). Recently we demonstrated that computational assistance might simplify the clinical DBS programming process and improve therapeutic outcomes (3). Given the expanded parameter search space of DBS devices with current steering capabilities, we propose that patient-specific computer models may be necessary to exploit the full potential of current steering technology.

Study limitations

The technical limitations of the DBS computational models used in this study are well documented in our previous work (12, 16, 20). Principal limitations specific to this study relate to the representation of the specific neural populations. Among the three different neural populations that were studied, only one (IC axons) could be reconstructed directly from streamline tractography. However, DTI tractography only provides a rough estimate of individual axon trajectories. The other two populations were reconstructed based on non-human primate staining studies of individual neurons. Therefore, subtle differences in the activation percentages for all of the different neural populations could result from the nuances within our specific trajectories. Despite these caveats, our implementation combined use of detailed anatomical and electrical models to directly stimulate these neural populations, and determine which ones were active for a given stimulation parameter setting. This population based analysis allowed us to account for subtle geometrical differences in the position/orientation of neurons relative to the DBS electrode. It should also be noted that this theoretical study was performed as a proof-of-concept and not intended to be specific to any individual patient.

Another limitation of this study was that much of the analysis was performed at a single electrode location. Many different electrode positions/orientations are encountered in clinical practice, which would affect the selectivity for each neural population. However, this study does show that current steering can selectively activate different proportions of target neural populations when the electrode is implanted in a clinically relevant region.

For the purposes of standardization across the different neural populations, we used a common axon diameter for each neuron type. In reality, each neuron type has a range of axon diameters associated with it, and the distribution of diameters differs between the neuron types. Unfortunately, histological documentation of these measurements is limited. However, it is likely that on a relative scale between our three populations, the IC would be associated with larger diameter fibers, while the STN and GPi would be associated with smaller diameter fibers. This would bias stimulation thresholds toward the IC and should be noted when interpreting our results.

Another caveat of this study was the definition of the entire STN population as a therapeutic target. The STN is known to consist of limbic, associative, and sensorimotor regions, and

therapeutic stimulation is commonly associated only with the latter. However, given the uncertainty of defining borders between these different regions, we elected to evaluate the STN as a single entity for simplicity in this proof-of-concept study. Still, we focused our analysis on electrode locations in the dorsal STN, which is the general region associated with the sensorimotor area.

Conclusion

While typical clinical practice with traditional DBS technology tends to focus on monopolar stimulation, we found that DBS devices capable of current steering between contacts opens up additional opportunities to achieve an improved balance between activation of target and side-effect neural populations. This study demonstrated that increased selective activation was possible by using a current-controlled device with independent sources. Future studies are needed to explicitly define the therapeutic target(s) for stimulation, as well as to investigate other lead trajectories and electrode contact designs that may provide greater selectivity between those targets.

Acknowledgments

This work was supported by the National Institutes of Health (R01 NS059736) and Boston Scientific Neuromodulation Corporation.

References

1. Obeso JA, Olanow CW, Rodriguez-Oroz MC, Krack P, Kumar R, ELA. Deep-brain stimulation of the subthalamic nucleus or the pars interna of the globus pallidus in Parkinson's disease. The New England journal of medicine. 2001 Sep 27; 345(13):956–63. [PubMed: 11575287]
2. Weaver FM, Follett K, Stern M, Hur K, Harris C, Marks WJ Jr, et al. Bilateral deep brain stimulation vs best medical therapy for patients with advanced Parkinson disease: a randomized controlled trial. JAMA. 2009 Jan 7; 301(1):63–73. [PubMed: 19126811]
3. Frankemolle AM, Wu J, Noecker AM, Voelcker-Rehage C, Ho JC, Vitek JL, et al. Reversing cognitive-motor impairments in Parkinson's disease patients using a computational modelling approach to deep brain stimulation programming. Brain. 2010 Jan 7.
4. Butson CR, McIntyre CC. Current Steering to Control the Volume of Tissue Activated During Deep Brain Stimulation. Brain Stimulat. 2008 Jan; 1(1):7–15.
5. Khan MF, Mewes K, Gross RE, Skrinjar O. Assessment of brain shift related to deep brain stimulation surgery. Stereotactic and functional neurosurgery. 2008; 86(1):44–53. [PubMed: 17881888]
6. Pallavaram S, Dawant BM, Remple MS, Neimat JS, Kao C, Konrad PE, et al. Effect of brain shift on the creation of functional atlases for deep brain stimulation surgery. Int J Comput Assist Radiol Surg. 2010 May; 5(3):221–8. [PubMed: 20033503]
7. Walter U, Wolters A, Wittstock M, Benecke R, Schroeder HW, Muller JU. Deep brain stimulation in dystonia: sonographic monitoring of electrode placement into the globus pallidus internus. Mov Disord. 2009 Jul 30; 24(10):1538–41. [PubMed: 19489070]
8. Winkler D, Tittgemeyer M, Schwarz J, Preul C, Strecker K, Meixensberger J. The first evaluation of brain shift during functional neurosurgery by deformation field analysis. Journal of neurology, neurosurgery, and psychiatry. 2005 Aug; 76(8):1161–3.
9. Hunsche S, Sauner D, Maarouf M, Poggenborg J, Lackner K, Sturm V, et al. Intraoperative X-ray detection and MRI-based quantification of brain shift effects subsequent to implantation of the first electrode in bilateral implantation of deep brain stimulation electrodes. Stereotactic and functional neurosurgery. 2009; 87(5):322–9. [PubMed: 19713732]
10. Lempka SF, Johnson MD, Miocinovic S, Vitek JL, McIntyre CC. Current-controlled deep brain stimulation reduces in vivo voltage fluctuations observed during voltage-controlled stimulation. Clin Neurophysiol. 2010 May 19.

11. Lempka SF, Miocinovic S, Johnson MD, Vitek JL, McIntyre CC. In vivo impedance spectroscopy of deep brain stimulation electrodes. Journal of neural engineering. 2009 Aug.6(4):046001. [PubMed: 19494421]
12. Butson CR, Cooper SE, Henderson JM, McIntyre CC. Patient-specific analysis of the volume of tissue activated during deep brain stimulation. NeuroImage. 2007 Jan 15; 34(2):661–70. [PubMed: 17113789]
13. Wakana S, Jiang H, Nagae-Poetscher LM, van Zijl PC, Mori S. Fiber tract-based atlas of human white matter anatomy. Radiology. 2004 Jan; 230(1):77–87. [PubMed: 14645885]
14. Tuch DS, Wedeen VJ, Dale AM, George JS, Belliveau JW. Conductivity tensor mapping of the human brain using diffusion tensor MRI. Proceedings of the National Academy of Sciences of the United States of America. 2001 Sep 25; 98(20):11697–701. [PubMed: 11573005]
15. McIntyre CC, Mori S, Sherman DL, Thakor NV, Vitek JL. Electric field and stimulating influence generated by deep brain stimulation of the subthalamic nucleus. Clin Neurophysiol. 2004 Mar; 115(3):589–95. [PubMed: 15036055]
16. Miocinovic S, Parent M, Butson CR, Hahn PJ, Russo GS, Vitek JL, et al. Computational analysis of subthalamic nucleus and lenticular fasciculus activation during therapeutic deep brain stimulation. Journal of neurophysiology. 2006 Sep; 96(3):1569–80. [PubMed: 16738214]
17. Sato F, Parent M, Levesque M, Parent A. Axonal branching pattern of neurons of the subthalamic nucleus in primates. J Comp Neurol. 2000 Aug 14; 424(1):142–52. [PubMed: 10888744]
18. Parent M, Parent A. The pallidofugal motor fiber system in primates. Parkinsonism Relat Disord. 2004 Jun; 10(4):203–11. [PubMed: 15120094]
19. Weinstein, D.; Kindlmann, G.; Lundberg, E., editors. Visualization ‘99. IEEE; 1999 Oct 24–29. Tensorlines: advection-diffusion based propagation through diffusion tensor fields.
20. Chaturvedi A, Butson CR, Lempka SF, Cooper SE, McIntyre CC. Patient-specific models of deep brain stimulation: Influence of field model complexity on neural activation predictions. Brain Stimulat. 2010; 3(2):65–77.
21. McIntyre CC, Richardson AG, Grill WM. Modeling the excitability of mammalian nerve fibers: influence of after potentials on the recovery cycle. Journal of neurophysiology. 2002 Feb; 87(2): 995–1006. [PubMed: 11826063]
22. McIntyre CC, Grill WM. Excitation of central nervous system neurons by nonuniform electric fields. Biophysical journal. 1999 Feb; 76(2):878–88. [PubMed: 9929489]
23. Nowak LG, Bullier J. Axons, but not cell bodies, are activated by electrical stimulation in cortical gray matter. II. Evidence from selective inactivation of cell bodies and axon initial segments. Exp Brain Res. 1998 Feb; 118(4):489–500. [PubMed: 9504844]
24. Nowak LG, Bullier J. Axons, but not cell bodies, are activated by electrical stimulation in cortical gray matter. I. Evidence from chronaxie measurements. Exp Brain Res. 1998 Feb; 118(4):477–88. [PubMed: 9504843]
25. Foutz TJ, McIntyre CC. Evaluation of novel stimulus waveforms for deep brain stimulation. Journal of neural engineering. 2010 Dec.7(6):066008. [PubMed: 21084732]
26. Hines ML, Carnevale NT. The NEURON simulation environment. Neural computation. 1997 Aug 15; 9(6):1179–209. [PubMed: 9248061]
27. McIntyre CC, Grill WM. Extracellular stimulation of central neurons: influence of stimulus waveform and frequency on neuronal output. Journal of neurophysiology. 2002 Oct; 88(4):1592–604. [PubMed: 12364490]
28. Plaha P, Ben-Shlomo Y, Patel NK, Gill SS. Stimulation of the caudal zona incerta is superior to stimulation of the subthalamic nucleus in improving contralateral parkinsonism. Brain. 2006 Jul; 129(Pt 7):1732–47. [PubMed: 16720681]
29. Lee KH, Blaha CD, Harris BT, Cooper S, Hitti FL, Leiter JC, et al. Dopamine efflux in the rat striatum evoked by electrical stimulation of the subthalamic nucleus: potential mechanism of action in Parkinson’s disease. The European journal of neuroscience. 2006 Feb; 23(4):1005–14. [PubMed: 16519665]
30. Gradinaru V, Mogri M, Thompson KR, Henderson JM, Deisseroth K. Optical deconstruction of parkinsonian neural circuitry. Science. 2009 Apr 17; 324(5925):354–9. [PubMed: 19299587]

31. Xu W, Miocinovic S, Zhang J, Baker K, McIntyre CC, Vitek JL. Dissociation of motor symptoms during deep brain stimulation of the subthalamic nucleus in the region of the internal capsule. Exp Neurol. 2010 Aug 14.

32. Merrill DR, Bikson M, Jefferys JG. Electrical stimulation of excitable tissue: design of efficacious and safe protocols. J Neurosci Methods. 2005 Feb 15; 141(2):171–98. [PubMed: 15661300]

33. Moro E, Poon YY, Lozano AM, Saint-Cyr JA, Lang AE. Subthalamic nucleus stimulation: improvements in outcome with reprogramming. Arch Neurol. 2006 Sep; 63(9):1266–72. [PubMed: 16831958]

34. McIntyre CC, Miocinovic S, Butson CR. Computational analysis of deep brain stimulation. Expert Rev Med Devices. 2007 Sep; 4(5):615–22. [PubMed: 17850196]

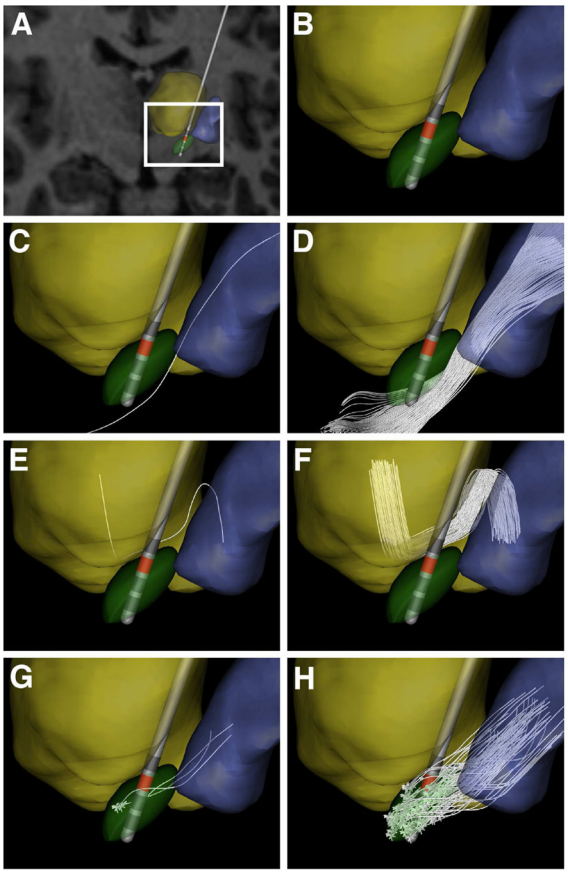

Fig 1.

Anatomical model. (A) MRI brain atlas with a typical electrode position for STN-targeted DBS, along with relevant nuclei (thalamus – yellow volume; STN – green volume; GP – blue volume). (B) Zoomed-in version of the nuclei and electrode position. (C) A single IC axon defined via tractography. (D) 200 unique IC axon trajectories reconstructed from a seed region just lateral to the STN. (E) A single GPi axon passing through the lenticular fasciculus. (F) The initial axon trajectory was randomly copied within a predetermined region of interest to create a GPi bundle consisting of 80 fibers. (G) Three different STN neurons (including dendrites, soma, and axon). (H) These three initial neurons were replicated within the STN nuclei boundaries to create 100 total STN projection neurons.

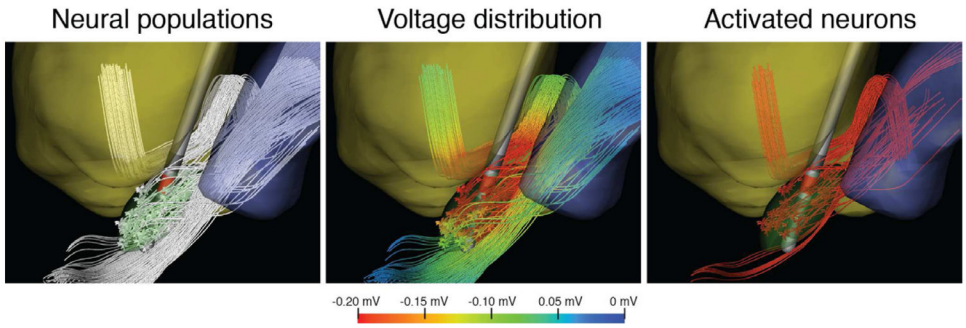

Fig 2.

Neural activation during typical monopolar stimulation. (A) Contact 2 was an active cathode at −6 mA. (B) Extracellular voltage distribution for all three neural populations during stimulation. (C) After running neural simulations, we observed that 62% of the GPi axons, 43% of the STN projection neurons, and 5% of the IC axons were activated.

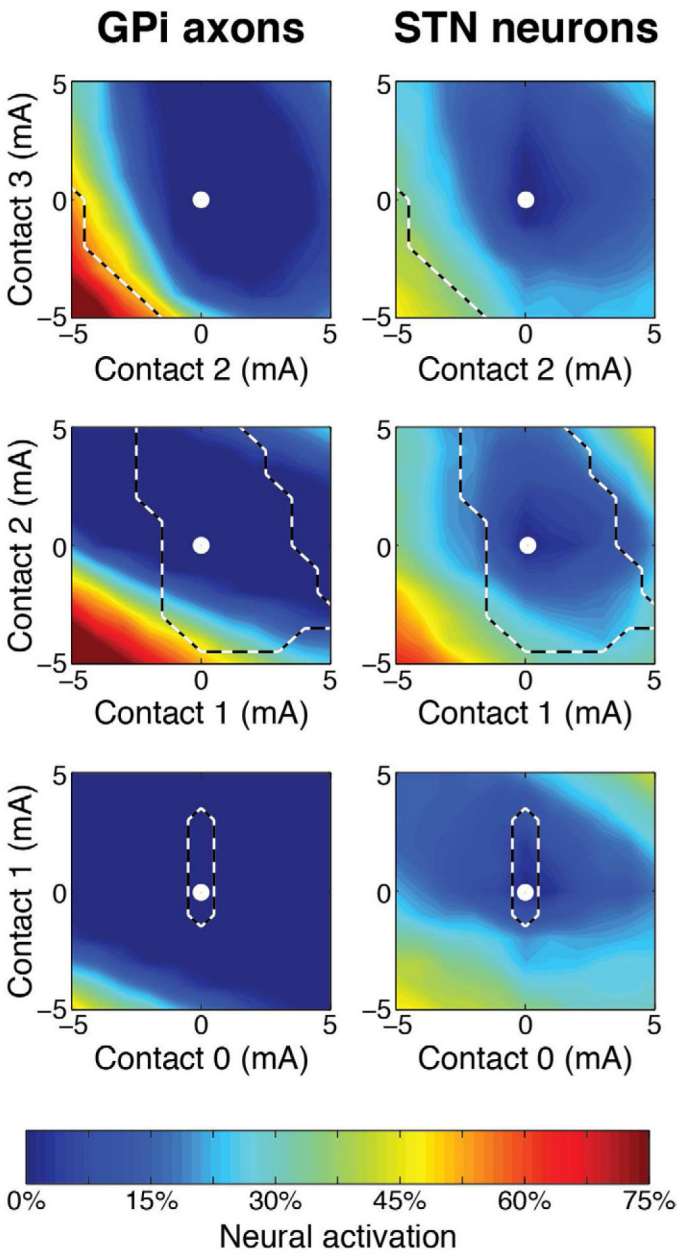

Fig 3.

Neural population recruitment during bipolar current steering. Spatial activation is shown for each of the two therapeutic neural populations in response to all combinations of adjacent bipolar contact configurations. Stimulation settings within the dashed lines describe no internal capsule activation. The stimulation amplitudes ranged from maximum anodic (−5 mA) to maximum cathodic (+5 mA), with an amplitude resolution of 1 mA. The white dot in the center of the image describes no stimulation.

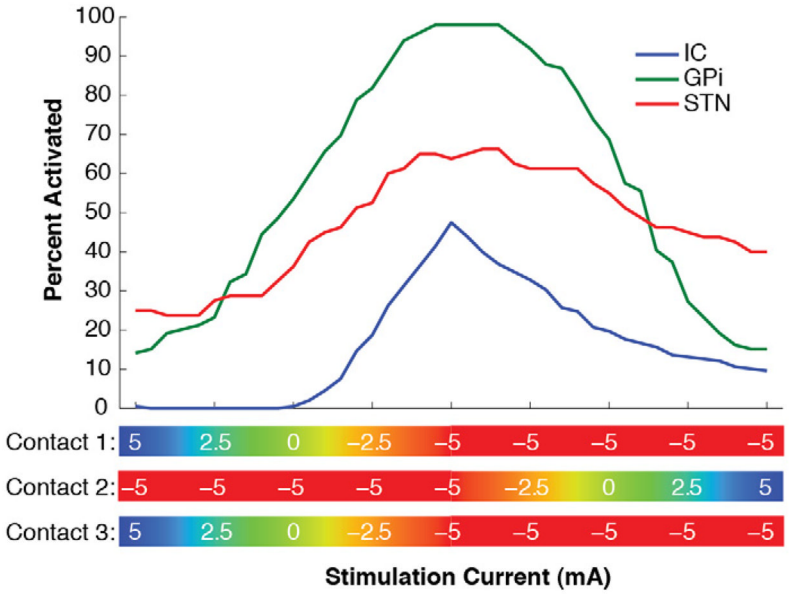

Fig 4.

Neural activation during current steering using a tripolar configuration of contacts 1–3. Associated neural activation profiles are shown while each contact was varied individually between the cathodic −5 mA and the anodic +5 mA stimulation amplitudes.

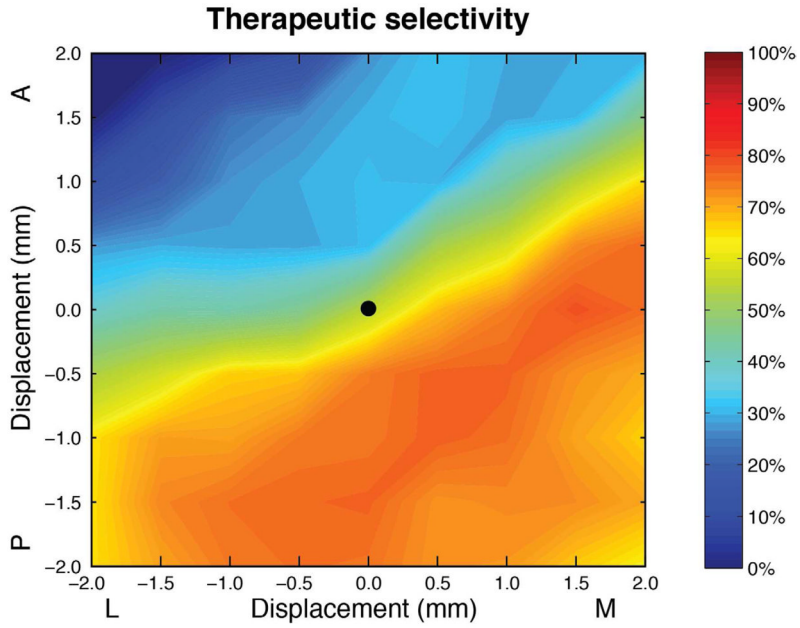

Fig 5.

Contour map depicting the maximum average selective activation of both therapeutic neural populations (STN projection neurons and GPi axons) with no internal capsule activation, using ± 5 mA (1 mA increments) bipolar stimulation settings steered between contacts 2 and 3. This metric was defined as the combined maximum average of the percent of STN neurons and GPi axons groups individually activated. We perturbated the DBS electrode ± 2 mm (0.5 mm increments) in the mediolateral (x-axis) and anteroposterior (y-axis) directions. The black dot in the center of the image depicts the default electrode location.

Table 1

Maximizing the average selective activation of the neural populations below IC threshold. There were no stimulation settings that exclusively activated GPi. The combined columns depict the maximal total activation of both GPi and STN concurrently. Each average activation percentage is followed by the standard error of the mean. The individual stimulation settings that achieved those activations are listed within brackets.

	Neural populations activated (%) [stimulation setting] (mA)		
		Combined	
Stimulation type	**STN only**	**GPi**	**STN**
One contact (single source)	10.0 ± 1.2 [0, 0, 0, −2]	39.2 ± 3.9 [0, 0, −4, 0]	46.8 ± 4.8
Two contacts (single source)	25.2 ± 3.0 [0, −1, −1, 0]	44.7 ± 4.0 [0, 0, −3, −3]	50.8 ± 4.2
Two contacts (two independent sources)	33.5 ± 3.1 [0, −2, 4, 0]	50.7 ± 3.1 [0, 0, −4, −2]	55.1 ± 4.4